Soft Matter

Accepted Manuscript

ROYAL SOCIETY OF CHEMISTRY

www.rsc.org/softmatter

Soft Matter

RSCPublishing

ARTICLE

Stabilization and fabrication of microbubbles: applications for medical purposes and functional materials

Cite this: DOI: 10.1039/x0xx00000x

Received 00th xxx xxx,
Accepted 00th xxx xxx

DOI: 10.1039/x0xx00000x

www.rsc.org/

Mina Lee[a], Eun Yeol Lee[a], Daeyeon Lee[b]*, and Bum Jun Park[a]*

Microbubbles with diameters ranging from a few micrometers to tens of micrometers have garnered significant attention in various applications including food processing, water treatment, enhanced oil recovery, surface cleaning, medical purposes, and material preparation fields with versatile functionalities. A variety of techniques have been developed to prepare microbubbles such as ultrasonication, excimer laser ablation, high shear emulsification, membrane emulsification, an inkjet printing method, electrohydrodynamic atomization, template layer-by-layer deposition, and microfluidics. Generated bubbles should be immediately stabilized via the adsorption of stabilizing materials (e.g., surfactants, lipids, proteins, and solid particles) on the gas-liquid interface to lower the interfacial tension. Such adsorption of stabilizers prevents coalescence between the microbubbles and also suppresses gas dissolution and resulting disproportionation caused by the presence of the Laplace overpressure across the gas-liquid interface. Herein, we comprehensively review three important topics of microbubbles: stabilization, fabrication, and applications.

Introduction

After Claude R. Joyner accidently observed the contrast enhancement of an ultrasound signal after the injection of dye into a patient's ventricle in the late 1960's, it was later revealed that the contrast enhancement stems from the temporary formation of microbubbles formed at the catheter tip.[1, 2] Since this observation, studies of bubbles or microbubbles have been carried out for medical purposes[3-31] and further extended to applications in various fields such as food processing,[32-36] water treatment,[37, 38] enhanced oil recovery,[39, 40] geogas transportation phenomena,[41-43] surface cleaning,[44-46] and lightweight materials with versatile functionalities.[47-56]

A variety of techniques have been developed to prepare microbubbles with diameters ranging from a few micrometers to tens of micrometers.[57] Productivity and size uniformity of the bubble generation depend on the nature of these techniques. High yield production is advantageous for cost reduction via large-scale manufacturing, whereas size tunability is an essential factor particularly for therapeutic applications of microbubbles. Stochastic approaches offer a promising fabrication route with the benefit of large-scale generation of microbubbles. For instances, ultrasonication,[10, 58-61] excimer laser ablation,[62] or high shear emulsification[61, 63-65] generate turbulent flows that lead to the formation of stable bubbles. These stochastic methods, however, inevitably sacrifice the tunability of the bubble size and distribution. A microfluidic approach represents the opposite extreme and enables the generation of microbubbles with high uniformity which can be readily controlled by the flow rates of fluid streams, the physical and chemical properties of the fluids, and the geometry of microfluidic devices.[66-80] This method is also advantageous in imparting various functionalities to the bubbles, for example, by introducing functional nanoparticles in the bubble shell.[81-86] One critical limitation of microfluidic approaches is their relatively low productivity, which may be overcome by parallel connection and operation of multiple devices. Membrane emulsification is an intermediate approach between the two extremes, yielding moderate productivity without significantly sacrificing size uniformity.[56, 87-90] In addition, inkjet printing,[91] coaxial electrohydrodynamic atomization,[92-94] and colloidal templating incorporated in a layer-by-layer deposition method[95-105] offer alternative routes to generate microbubbles.

The controlled stability of bubbles is a crucial factor in practical applications.[106-109] For example, microbubbles used for medical applications should circulate through blood vessels over a desired period of time until they are no longer needed.[3] Various factors influence the bubble stability including the gas composition/solubility, medium conditions, and stabilizers. In particular, stabilizing materials, such as surfactants, lipids, proteins, and solid particles, adsorb onto the bubble-liquid interface, lowering the interfacial tension and thus, stabilizing the interface. However, gas dissolution can occur due to the

Laplace pressure across the gas-liquid interface, which can lead to disproportionation via Ostwald ripening. Suppression of the disproportionation process is the one of the most challenging issues in microbubble applications.

In this review, we comprehensively present three important topics of microbubbles: stabilization, fabrication, and applications. First, we focus on discussing the controlled stability of microbubbles in terms of preventing or retarding disproportionation or coalescence, depending on fluid environments, rheological properties, and the kinds of stabilizers/additives. Second, we review recent developments in a variety of microbubble preparation techniques, such as stochastic methods, forced extrusion methods, template layer-by-layer deposition, and microfluidic approaches. Last, we present applications for medicine and functional materials in which the dimensions of the microbubbles and a narrow size distribution are critical requirements.

Microbubble Stabilization

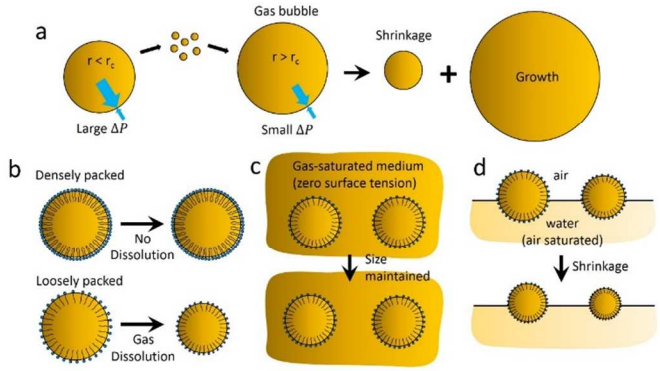

Fig 1. Schematics of bubble stability: (a) Ostwald ripening, (b) effect of molecular packing at the bubble-liquid interface, (c) suppression against disproportionation in a gas-saturated medium, and (d) bubble shrinkage in an open system.

Long-term or controlled stability is a critical requirement in many applications, whereas the stabilization of bubbles is not always desirable, for example, in defoaming processes. Surfactant, lipid, or protein molecules are representative molecular stabilizers that densely assemble to a gas-liquid interface. Once the interface is completely saturated by molecular stabilizers, the interfacial tension significantly decreases, ideally equalizing the pressures internal and external to the bubbles. This condition suppresses the Laplace pressure across the gas-liquid interface which induces a disproportionation process, imparting enhanced bubble stability. However, such coating materials can rarely be maximally compressed such that the Laplace overpressure leads to gas exchange between bubbles and thus, gradually broadens the size distribution (Fig. 1a and 1b).

Control of the disproportionation process is the one of the most important challenges in a variety of bubble applications.[106, 110] When bubbles are densely packed in either open or closed systems, the disproportionation process is very complicated and it is challenging to describe the mechanism using theoretical models because multi-body effects are likely to be important. Thus, to date, efforts have been mainly focused on understanding the fundamental mechanisms related to the stability of bubbles and the evolution of their size distribution in various model systems. The simplest model system involves isolated bubbles evenly dispersed in a closed container at a dilute volume fraction. The change of the size of these bubbles can be determined by the Laplace pressure, which is the difference between the pressures inside and outside of a bubble, expressed as $\Delta P = 2\gamma/r$, where γ is the interfacial tension and r is the bubble radius. The gas diffusion driven by this pressure difference promotes a change of the bubble size, such that smaller bubbles shrink and larger bubbles grow at the expense of the shrinkage of the smaller ones (Fig. 1a).

For a closed system in which the total amount of gas is conserved, the classical Lifshitz-Slyozov-Wagner (LSW) theory of Ostwald ripening can adequately capture the evolution of the bubble size distribution.[111, 112] In this case, each bubble is assumed to be isolated such that the diffusion flux of gas from the inside of a bubble toward a continuous medium dominantly depends on the presence of neighboring bubbles, accompanying the concentration change in the continuous medium over time. The corresponding time-dependent size distribution predicted by the LSW theory can be defined by universal scaling behavior given by $n(r,t) = N(t)f(r/r_c(t))$ where N is the total number of bubbles and r_c is the critical bubble radius.[111-113] The function $f(x)$ with a cut-off ratio of x = 1.5 indicates that the bubble radius does not exceed 1.5 times the average radius ($\langle r \rangle$) in the system. The critical radius (r_c) determines the growth or shrinkage of bubbles in which bubbles with a radius larger than r_c grow, bubbles with a radius smaller than r_c shrink, and bubbles with a radius equal to r_c neither grow nor shrink.

The LSW theory has been extended to a closed system with a finite volume fraction in which individual bubbles are no longer isolated but their spatial distribution is assumed to be uniform.[114-116] In this case, the growth and shrinkage of bubbles generally depend on the presence of their surrounding bubbles in a collective manner. The disproportionation process between lipid-stabilized bubbles with a finite volume fraction can be suppressed in an aqueous medium that is pre-saturated with air (Fig. 1c).[73] In this case, the initial size distribution of highly monodisperse microbubbles generated by a flow-focusing microfluidic device is maintained over significantly increased time periods. This suppression against disproportionation is likely because the interfacial tension between the gas and the medium pre-saturated with the gas significantly reduces, resulting in halting the gas dissolution through the medium. Similarly, for an open system where the continuous medium containing bubbles is exposed to atmospheric conditions (e.g., air-water interface), evolution of the bubble size distribution is not significantly affected by the presence of surrounding bubbles since the bulk phase is saturated with gas (i.e., air) and the gas concentration in the bulk is constant (Fig. 1d).[110] Accordingly, the Laplace overpressure subjected on each bubble at the interface likely leads to consistent shrinkage of the bubbles.

Interestingly, for an open system in which bubbles located beneath a planar air-water interface are sufficiently separated from each other, it was experimentally observed that the rheological properties (e.g., viscosity and elasticity) of the bubble surface do not significantly influence the disproportionation behavior.[117] The bubbles are stabilized by several proteins such as whey protein isolate, sodium caseinate, gelatin, and pure β-lactoglobulin, where each protein alters the viscoelasticity of the bubble-liquid interface. Upon contacting the planar air-water interface, bubbles stabilized with different proteins shrink without showing significant variations of the size shrinkage kinetics. In this particular system, diffusion between the bubbles and through the continuous medium was found to be a critical factor in determining the observed evolution. In general, however, the interfacial rheological properties would influence the bubble stability because coating materials adsorbed to the bubble-liquid interface form a steric barrier for gas molecule diffusion, possibly retarding or preventing the disproportionation process.[115, 118] For instance, the presence of stabilizers such as surfactants or amphiphilic polymers decreases the interfacial tension and thus, stabilizes bubbles dispersed in a bulk medium. Upon increasing or decreasing the bubble size via the disproportionation or coarsening process, the interfacial tension will vary if additional adsorption or desorption of the stabilizers does not occur. The interfacial tension has a proportional relationship to the capillary length that consequently affects coarsening.[115] In addition to the effect of the interfacial rheological properties (i.e., interfacial elasticity and interfacial viscosity), bulk rheological properties (i.e., viscosity and shear modulus) also influence the dissolution behavior of a bubble.[118] It has been reported that stability criteria in which gas dissolution is halted can be defined by either the interfacial elasticity or bulk elastic modulus, whereas the bulk and interfacial viscosity cannot stop the dissolution process but can only retard the dissolution.[118]

The electrolyte concentration can also play an important role on the bubble stability because the intermolecular interactions and packing fraction between surface coating materials are highly susceptible in the presence of the electrolyte in a bulk medium, consequently altering the rheological properties of the interface. For instance, the size distribution and stability of microbubbles have been investigated by varying the concentration of a surfactant (sodium dodecyl sulfates, SDS) and electrolyte (sodium chloride).[119] As the SDS concentration increases, the bubble size was found to decrease and the maximum stability was obtained above the critical micelle concentration (CMC) of SDS (i.e., 3.5mM measured in this work). It was also found that the addition of electrolyte and SDS (below the CMC) in the bubble generation lowers the surface tension, leading to a reduction of the bubble size and enhancement of the bubble stability. The presence of electrolyte likely decreases the electrostatic repulsion between the polar head groups of the SDS molecules and, consequently, SDS molecules lead to the formation of a closely packed film at the bubble surface, resulting in lowering of the surface tension.

Solid particles can also stabilize bubbles preventing disproportionation and coalescence. A sonicated dispersion of hydrophobically-modified silica nanoparticles leads to spontaneous adsorption of the particles to the air-water interface in an aqueous solution containing an electrolyte (i.e., sodium chloride).[120] Such particle-stabilized bubbles, so-called armored bubbles, were found to be extremely stable at high salt concentrations (i.e., 0.5–3.0 M NaCl), in which the particles form a weak gel at the air-water interface with a finite yield stress that increases with increasing salt concentration.

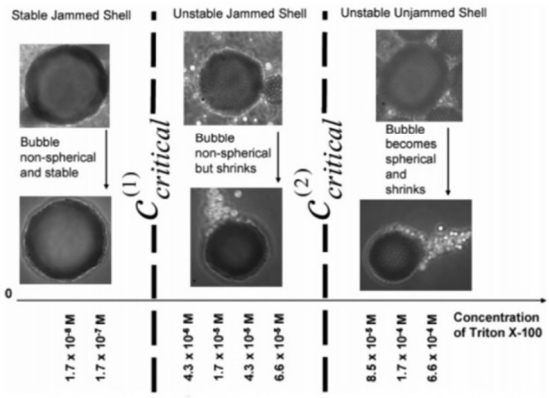

Fig 2. Effect of Triton X-100 surfactant on the stability of armored bubbles. Reprinted from ref. 121 with permission.

The presence of surfactant molecules can affect the stability of armored bubbles. Air bubbles stabilized by solid particles can be prepared either by a microfluidic flow-focusing method or by manually and vigorously shaking an aqueous suspension of the particles.[121, 122] The resulting air bubbles were found to be stable against coalescence and the shape of the bubbles was nonspherical, indicating jamming of the particles at the interface.[122] When an isolated stable armored bubble is exposed to the CMC (ca. 0.2 mM) of a surfactant (i.e., Triton X-100), the bubble immediately becomes spherical and the particles (i.e., polystyrene) at the air-water interface simultaneously detach from the interface.[121] The particles remaining at the spherical air bubble surface organize into a hexagonal structure with a finite interparticle distance and consequently, the bubbles proceed to dissolve. This behavior over this concentration regime ($c > c^{(2)}_{critical}$ in Fig. 2) can be attributed to the adsorption of surfactant molecules onto the particle surface and the air-water interface, changing the wettability of the particles and the microstructure of the interfacial particles. In contrast, upon exposure of the jammed nonspherical bubble to a surfactant concentration below the CMC ($c^{(1)}_{critical} < c < c^{(2)}_{critical}$in Fig. 2), the isolated bubble remains nonspherical while ejecting the particles from the interface until it disappears completely by dissolving. In this intermediate regime of the surfactant concentration, the interfacial jamming and stresses on the particle-covered shell may play important roles in the bubble dissolution and destabilization process (Fig. 2). In short, prior to the use of bubbles, it is essential to screen various kinds of

coating materials, gas compositions, and fluid media to achieve a desired stability suitable for particular applications.

Fabrication

Stochastic method. Microbubbles can be generated by ultrasonication, excimer laser ablation, or high shear emulsification methods. These methods are advantageous because of their high yield and low cost of production. Sonochemistry is the most common method that allows for the one-step preparation of microbubbles.[10, 58-61] When high-intensity ultrasound is introduced to a solution that contains coating materials or surfactants, acoustic cavitation occurs and the subsequent adsorption of such surface active materials stabilizes the gas-liquid interface. For example, the introduction of high-intensity ultrasound leads to chemical modification of lysozyme molecules in an aqueous solution, which are subsequently adsorbed and form a cross-linked layer at the bubble-liquid interface.[59] It is interesting to note that this ultrasound-induced emulsification and simultaneous cavitation/stabilization by the enzyme molecule produce microbubbles which are responsive to enzymatic activities.

Similar to the sonochemistry-based microbubble generation method, excimer laser ablation can produce microbubbles.[62] In this technique, an excimer laser with a wavelength of 248 nm is focused onto the surface of solid aluminum (Al) in water and, consequently, Al species are oxidized forming Al_2O_3 nanoclusters. The laser ablation also produces bubbles at the solid-liquid interface that capture Al_2O_3 nanoclusters onto the gas-liquid interface, stabilizing the gas bubbles. Since the resulting bubble size is controlled by stochastic processes (i.e., ultrasonication and laser ablation), these methods inevitably lead to bubbles with a broad size distribution. Therefore, an additional separation process is required to remove the large bubbles if the application involves injection into animals or human body.[57, 58]

Another method that allows for the large-scale generation of microbubbles is to use a high shear flow to emulsify gas (i.e., dispersed phase) or liquid in an aqueous continuous phase that contains a stabilizer.[61, 63-65] Adsorption of the stabilizer to the interface between the dispersed and continuous phases occurs under the high shear flow, forming stabilizer-coated gas bubbles in the aqueous phase. In certain cases, a volatile organic solvent is mixed with the aqueous phase to dissolve a non-water soluble polymer, which eventually attaches to the interface between the gas and water phases to stabilize the microbubbles. When a liquid is used as the disperse phase, such emulsion droplets can be converted to microbubbles by freeze-drying. This high shear emulsification leads to the generation of microbubbles with a broad size distribution.

Forced extrusion methods. Membrane emulsification is a less energy intensive method compared to sonication and high shear emulsification, and can be used to generate microbubbles with a narrow size distribution for moderate-scale production (Fig. 3a).[56, 87-90] A dispersed phase is forced through a porous membrane which possesses a suitable stiffness and wettability. The gas bubbles permeate through the pores of the membrane and disperse into the continuous phase flowing along the membrane surface. Such break-up events are influenced by experimental parameters, such as the shear stress of the continuous flow, the buoyancy force of the droplets or bubbles, the interfacial tension, and the applied pressure of the dispersed phase.[87, 90] The addition of emulsifiers is required to prevent coalescence among the generated gas bubbles. This method offers the advantage of controlling the size and size distribution of the bubbles by varying the experimental parameters such as flow velocity, transmembrane pressure difference, and the kinds of emulsifiers. In addition, the characteristics of the membrane, such as the pore size distribution and chemical/mechanical properties, have significant impacts on the bubble size. For example, as the contact angle on the surface-modified membranes decreases, the bubble size and size distribution decrease, as shown in Fig. 3b. Bubbles formed from the membrane pores with a hydrophilic surface (i.e., lower contact angles) easily detach from the membrane surface and consequently the bubble size is mainly determined by the membrane pore diameter. In contrast, good wettability of the gaseous phase to the hydrophobic surface (i.e., higher contact angles) leads to coalescence of bubbles prior to detachment of the bubbles from the membrane surface, resulting in relatively large size and a broad size distribution.

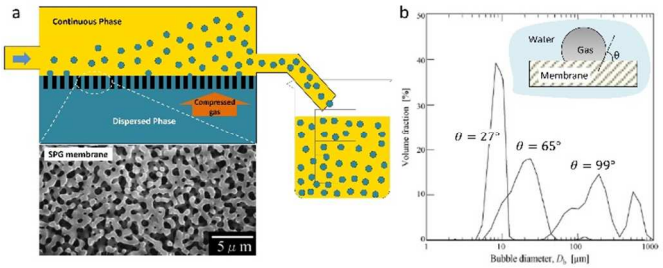

Fig 3. (a) Schematic of the experimental apparatus used for the membrane emulsification method. A scanning electron microscope (SEM) image of a Shirasu-porous-glass (SPG) membrane is shown on the bottom. (b) Effect of surface wettability of the membrane on the size and size distribution of bubbles. Modified and reprinted from ref. 89 with permission.

Microbubble fabrication with a high throughput and improved uniformity has also been demonstrated by employing an inkjet printing method (Fig. 4a and 4b).[91] Bubbles are formed by forcing a polymer solution through piezo-driven inkjet nozzles with diameters of 20, 30, and 50 μm. The pressure generated by the piezoelectric crystal creates pulses in the solution and each pulse leads to the formation of a droplet at the nozzle. Polymer capsules can be prepared by adding a non-solvent (e.g., cyclodecane) to the polymer (e.g., poly-(lactide-co-glycolide), PLGA) dissolved in a co-solvent (e.g., dichloromethane). Upon the removal of the co-solvent via drying, phase separation occurs such that the non-solvent and polymer form a core and shell, respectively, resulting in core-shell droplets with a narrow size distribution (closed circles in Fig. 4c). Subsequent freeze-drying of the samples leads to the

formation of gas-filled polymer capsules, maintaining the size uniformity (open circles in Fig. 4c). The capsule size can be readily controlled by varying the frequency and length of the pressure pulses. A moderate pressure is sufficient to produce droplets because the solvent is not forced to flow in a narrow orifice as is the case with membrane emulsification or microfluidic devices.

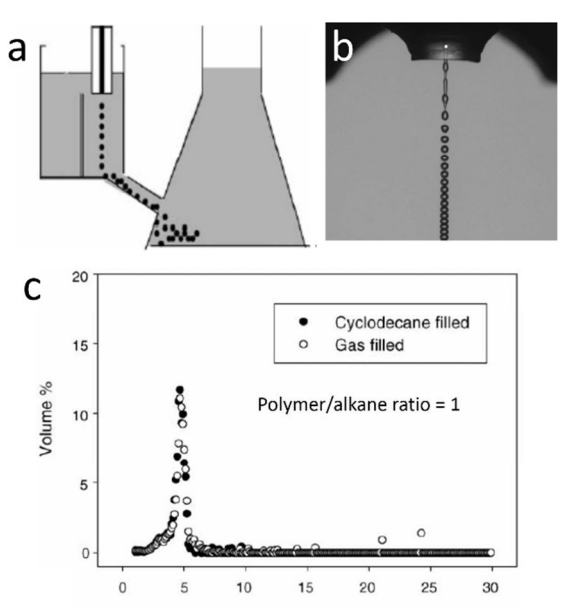

Fig 4. Inkjet printing method: (a) schematic illustration, (b) snapshot of droplet formation from piezo-driven inkjet nozzles, and (c) the size distribution of polymer capsules before and after freeze-drying. Modified and reprinted from ref. 91 with permission.

The electrohydrodynamic atomization method can provide a promising route to produce sub-10 μm microbubbles with a narrow size distribution in a single step (Fig. 5a).[92, 93] Two immiscible fluids (e.g., liquid and gas) supplied by a pair of syringe pumps are passed through two coaxially arranged needles. In the presence of an electric field, a coaxial jet of the two fluids is formed and atomization takes place to produce uniform droplets encapsulating gas pockets. An increase of the applied voltage reduces the diameter of the jet stream, resulting in the reduction of the microbubble size. The dimension of microbubbles is also affected by the flow rates of the inner (air) and outer (glycerol) phases. Based on the experimental results, the critical factor to achieve a relatively narrow size distribution of the generated microbubbles is the ratio of liquid to air flow rates that was found to be $n \sim 1.5$ (Fig. 5b). An advantageous feature of this method is that microbubbles with multi-layered coatings can be fabricated in a single step upon adding liquid coaxial streams in the jet mode.[94]

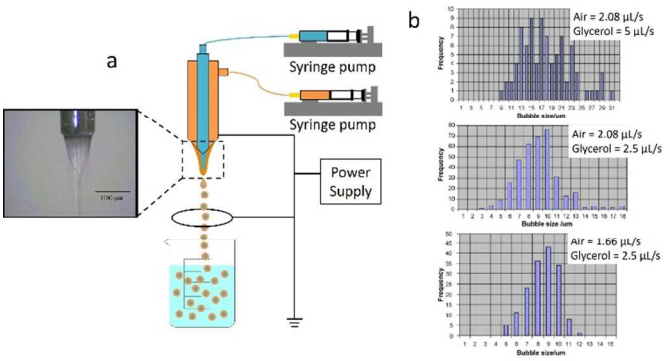

Fig 5. (a) Schematic of co-axial electrohydrodynamic atomization. (b) Size distribution of microbubbles depending on the flow rates of the inner phase (air) and the outer phase (glycerol). The applied voltage is 8.8 kV. Modified and reprinted from ref. 93 with permission.

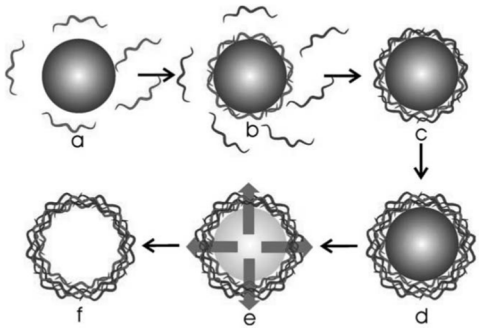

Fig 6. Schematic of the preparation of hollow capsules using the template LbL deposition method: (a-d) stepwise adsorption of oppositely charged macromolecules onto a template particle surface, (e) removal of the core template, and (f) the formation of the hollow-shelled structure. Reprinted from ref. 102 with permission from The Royal Society of Chemistry.

Template layer-by-layer deposition. Hollow microcapsules with a homogeneous size distribution can be fabricated by using layer-by-layer (LbL) assembly templated on various sacrificial core materials (Fig. 6).[95-105] For instance, suitable polymer particles are used as templates on which consecutive adsorption of oppositely charged polymers forms stable multilayers due to the strong electrostatic interactions between the anionic and cationic components. The polymer core is chemically removed under appropriate conditions (e.g., strong acidic solution) while the integrity of the polymer or polyelectrolyte complex is preserved, resulting in hollow-shelled structures. In general, the prepared core-shell capsules are not mechanically robust such that the structure easily collapses upon a small shear stress or bending resistance. Numerous methods have been developed to reinforce the mechanical strength of the shell based on a hydrogen-bonded assembly, polymerization, heat treatment, and nanoparticle adsorption.[97-99, 101, 103] This template LbL method can offer benefit of facile controllability of the size and size distribution of microcapsules that inherently depend on the dimension of the core template particles.

Microfluidics. Microfluidics have been used to generate microbubbles with precisely controlled dimensions. Their size

can be controlled by the flow rate and viscosity of liquids, the pressure of the gas stream, and the orifice size.[66-86] To result in an extended lifetime, which is one of the essential factors for practical applications, the generated bubbles should be covered with suitable coating materials, such as surfactants, phospholipids, biopolymers, and nano-/micro-particles. Various polymers can significantly enhance the bubble stability against gas dissolution, disproportionation, and coalescence. For example, polymer-shelled bubbles have been generated by using a glass capillary-based microfluidic device with a flow-focusing geometry.[71] Nitrogen gas is supplied to an inlet capillary channel and a glassy biocompatible polymer solution (e.g., PLGA dissolved in chloroform) in a co-axial capillary channel encapsulating the gas stream. The gas in oil flowing out of the orifice hydrodynamically focuses with an aqueous continuous medium containing polymer surfactants (polyvinyl alcohol), breaking the stream into monodisperse air-in-oil-in-water compound bubbles with a core-shell structure. Polymer-shelled bubbles are then obtained upon removal of the solvent in the middle phase via evaporation under ambient conditions. This fabrication method is useful to quantitatively explore bubble stability which depends on the bubble radius and the thickness of the bubble shell. A similar approach has been used to produce multilayered bubbles (gas/liquid/liquid) of double emulsion types using a dual-coaxial microfluidic device or a combination of two different microfluidic geometries: the flow-focusing and the T-junction.[68, 70] In the presence of emulsifiers and polymerizable monomers in the middle phase, multiple gas pockets are stabilized in the core region and the middle phase can be readily polymerized for further practical applications.

A similar approach of generating small and monodispersed bubbles encapsulated with a biocompatible polymer shell was also reported by employing a microfluidic device that was prepared by a soft-lithographic method.[67, 77, 84, 123] A gas mixture of CO_2 and a small amount of water-insoluble gas is forced out of an orifice to initially generate micro-sized bubbles in an aqueous solution containing lysozyme and anionic polysaccharide (i.e., sodium alginate) (Fig. 7a and 7b). The size of the gas bubbles mainly comprised of CO_2 gas decreases in the flow channel due to its high solubility in water. Dissolution of CO_2 gas leads to a reduction of size and the simultaneous acidification of the aqueous solution in the vicinity of the bubbles. The pH change causes the deposition of lysozyme and polysaccharide at the gas-water interface due to the electrostatic interactions, eventually forming stable polymer shelled bubbles. A notable fact of this method is that the bubble size is controlled not only by the geometry of the microfluidic device and the gas/liquid flow rates, but also by the composition of the gas mixture (i.e., CO_2 content) and the fluid conditions (i.e., the concentration of lysozyme and polysaccharide in the aqueous phase). For instance, the initial diameter of the generated bubbles decreases as the flow rate of the aqueous phase increases and consequently the final size of the bubbles decreases (Fig. 7c). The increase in the concentration of alginate in the continuous phase leads to the increase in the viscosity of the medium, resulting in the reduction in the size of the initial and final bubbles (Fig. 7d).

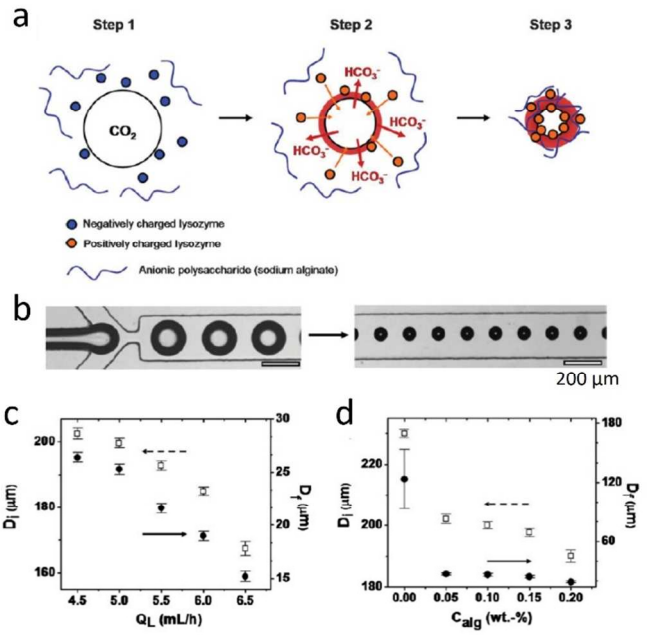

Fig 7. (a) Schematics of generating small and monodispersed bubbles encapsulated with a biocompatible polymer shell. (b) Microscopic snapshots indicate that the size of generated CO_2 bubbles decreases in the microchannel at a high pH condition. (c-d) Effect of the flow rate of the outer aqueous phase (c), and the concentration of alginate (d) on the bubble size. Modified and reprinted from ref. 77 with permission.

Solid particle stabilized-bubbles or armored bubbles are also extremely stable because the interfacial particles form a rigid layer, preventing dissolution of the gaseous phase.[83-85, 121, 122] Colloidal particle-shelled bubbles can be prepared by chemically directing the particle assembly at a gas-liquid interface in a microfluidic T-junction device that is fabricated in PDMS by using the soft lithography method.[84, 123] As CO_2 bubbles are generated in an aqueous solution (pH ≈ 14) containing anionic colloidal particles, the shrinkage of the bubbles immediately occurs due to the dissolution of CO_2 at high pH conditions. It was suggested that the acidity increase around the bubbles can chemically drive the particle adsorption on the gas-liquid interface, stabilizing the bubbles.

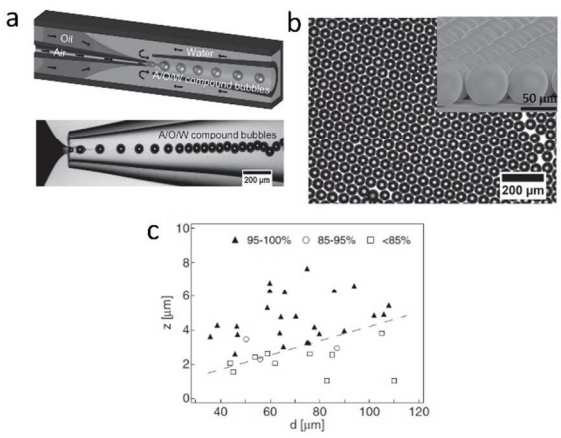

Fig. 8 (a) Generation of nanoparticle-shelled bubbles using the flow-focusing microfluidic device. (b) A microscopic snapshot of the generated microbubbles. The inset is an SEM image. (c) Stability state diagram depending on the dimension of microbubbles. Modified and reprinted from ref. 83 with permission.

Particle-stabilized bubbles with enhanced mechanical properties have been prepared by a glass capillary tube-based microfluidic device with a flow-focusing geometry (Fig. 8a and 8b). This method for the nanoparticle-shelled bubbles generation is quite similar to that for the polymer-shelled bubbles, except that the middle phase is composed of nanoparticles dispersed in a suitable volatile solvent.[71, 85] The stability of the generated bubbles against rupturing upon drying/re-suspending depends on the dimension of microbubbles that can be readily controlled by the flow rates of the three fluid streams entering the microfluidic device. In general, as the ratio of shell thickness (z) to bubble diameter (d) increases, the stability of nanoparticle-shelled bubbles against destruction increases in which the critical ratio was found to be $(z/d)_c \sim 0.042$ (Fig. 8c). This method is advantageous because the mechanical strength of nanoparticle-shelled bubbles can be readily tailored using thermal treatment while maintaining their ultra-light property. Silica nanoparticle-shelled bubbles treated by calcination and a sintering process have been quantitatively studied and have exhibited significantly increased elastic response and mechanical stiffness.[83] Notably, the unique feature of this method is that multicomponent bubbles can be generated by incorporating various functional materials in the oil phase which eventually form the shell. For example, magnetically responsive bubbles can be prepared by adding a small amount of magnetic nanoparticles in the oil phase containing silica nanoparticles.[85] Additionally, co-deposition of biopolymers and nanoparticles at the gas-liquid interface has been shown to result in the simple production of microbubbles with a narrow size distribution, long-term stability, and multi-functions stemming from the adsorption of various functional particles to the interface.[81] In short, the microfluidic generation of microbubbles provides the critical advantage of a highly uniform size. The shell functionalities of microbubbles can also be readily tuned by simply introducing functional materials (e.g., magnetic nanoparticles) in the middle phase that forms the shell. However, compared to other methods, the productivity of the microfluidics approach is relatively low.

Applications

Bubbles with micrometer dimensions have great potential for applications in various fields. For examples, ozone microbubbles have been used in water purification and sewage treatment processes.[38] Dissolved oxygen in aquatic environments is effectively increased by supplying oxygen as microbubbles. This system can be applied in aqua-farming and aerobic fermentation production facilities. Microbubble transportation phenomena have been used as a model system for geogas (i.e., radon) transport in water.[41-43] It was found that the upflow of geogas leads to the formation of microbubbles, efficiently carrying the geogas from deep sources to the water surface. Bubbles have also been importantly utilized in food processing.[32-36] For instance, the structure and stability of aerated food products are strongly affected by the type of gas. Air bubbles in solid foams (e.g., bread and snacks) and in liquid foams (e.g., whipped cream, coffee, and beer) are a significant factor to build the structure and to control taste, texture, and calories. In spite of these numerous applications in various fields, this section focuses on two major topics: applications for medicine and functional materials in which the dimensions of microbubbles and a narrow size distribution are critical requirements.

Medical applications. Microbubbles have provided great promise in diagnostic and therapeutic applications including ultrasound contrast agents, blood substitutes, targeted drug/gene delivery, and clot destruction.[3, 4, 6-13] For these biomedical applications of microbubbles, several important factors should be considered and required, such as long-term stability, biocompatibility, and controllability of the size with a narrow size distribution. These mechanical and chemical characteristics can be tuned by employing the coating materials and fabrication methods discussed previously.

Microbubbles are used as ultrasound contrast agents due to their high compressibility which enables them to efficiently scatter ultrasound. For example, ultrasound waves are reflected and scattered in the presence of interfaces between surrounding tissues and the gas in the microbubbles that are administered in a blood vessel. The resulting echogenicity mismatch increases the ultrasound backscatter generating a sonogram with an enhanced contrast which facilitates distinguishing the blood stream from the surrounding tissues. By incorporating the contrast-enhanced ultrasound to the targeted imaging modality, microbubbles equipped with ligands that bind molecular receptors on an organ in a circulatory system enable visualization of the area of interest.[20, 21] Once the microbubbles reach the targets and bind specifically, ultrasound can be utilized to convert the resulting echogenicity mismatch to a contrast-enhanced image of the area of interest. Differently, a destruction-replenishment method can be used in which the

microbubbles are destroyed by introducing ultrasound with a destructive pulse when they are in the region of interest.[29] The replenishment of the region with fragments of bubbles is used to efficiently image the area of interest upon subsequently supplying nondestructive pulses with a low pressure.

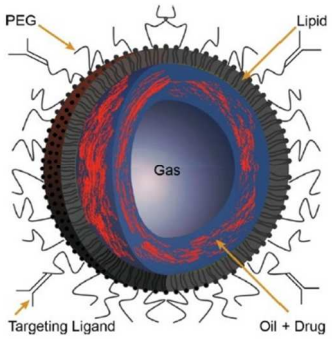

Fig. 9 Schematic of a multilayer microbubbles that can be applied in a site-specific delivery system. Reprinted from ref. 4 with permission.

Microbubbles composed of inner pockets and/or a shell are suitable for the site-specific delivery of drugs, genes, and oxygen that can be triggered by employing focused ultrasound (Fig. 9).[3-5] When drug-laden microbubbles freely circulating along a blood vessel reach a target site, supplying sufficiently strong ultrasound leads to the rupture of the bubbles accompanied by local release of the drug. This approach of the drug delivery using microbubbles can be extended to the targeted delivery based on the electrostatic/hydrophobic interactions or the ligand-receptor binding system.[14-28] Intravenous administration of drug-loaded microbubbles is locally concentrated in the target region and then destructive ultrasound pulses are employed to collapse the bubbles, locally liberating the drug. For example, it was reported that the negative surface charges on lipid-coated microbubbles enhance surface attachment to the capillary endothelium via complement-mediated interactions.[17] In contrast, the presence of a polyethyleneglycol (PEG) layer on the bubble shell that is often used as a protective layer of microbubbles reduces electrostatic and hydrophobic interactions between lipid membranes and the endothelium due to steric hindrance, and thus, inhibits capillary retention of the bubbles. Another targeted approach is the ligand-receptor system in which receptors specifically bind the ligands that are deliberately attached to the bubble surface. For instance, lipid-shelled microbubbles conjugated with monoclonal antibodies (MB_p) have shown enhanced attachment to tumor necrosis factor (TNF)-α-stimulated wild-type mice, compared to untreated wild-type mice.[22] It was also found that the microbubbles with the antibodies (MB_p) increase specific binding to P-selectin on endothelial cells, whereas the microbubbles without antibody (MB) and with isotype control antibody (MB_{iso}) did not significantly show increase in retention of microbubbles.

Applications for functional materials. Mechanically robust bubbles have been of great interest as an excellent candidate for the building blocks for lightweight materials to improve the energy efficiency of vehicles and equipment in various fields. In contrast, the flexibility and deformability of bubbles are essentially required for applications related to bendable devices, sound insulation materials, and impact absorbers. These functional materials can be fabricated by directed assembly, polymer foaming, and using composites of mechanically controlled bubbles with matrix components, such as mud, concrete, ceramic, polymer, and metals.

Composite materials consisting of microbubbles and a polymer matrix using a layer-by-layer approach provide a promising route for fabricating lightweight materials with controllable mechanical properties. As described, a variety of methods have been employed to prepare bubbles and considering control of the bubble size, one of the most efficient techniques is the microfluidic approach. Size tunable microbubbles with a high uniformity can be generated using flow-focusing microfluidics constructed with glass capillary tubes in which gas in oil in water compound bubbles are formed in the capillary channel and collected in a bulk aqueous medium.[85, 86] The middle oil phase is composed of silica nanoparticles dispersed in a volatile solvent and the outer water phase contains polymer surfactants to prevent coalescence between the bubbles. Upon evaporating the solvent in the middle phase, a thin and stiff nanoparticle shell is formed by the compaction of the particles, enabling the gas to be captured in the core. These microbubbles can be further modified using thermal treatment to impart desired mechanical properties (Fig. 10). Calcination at temperatures around 700°C leads to shell formation with porosity resulting from the removal of the residual polymer components on the shell surface, whereas a sintering process around 1200°C fuses silica particles, forming a dense and nonporous solid silica shell. Nanoindentation on a single bubble is commonly used to characterize the mechanical properties of these bubbles. When the as-assembled bubbles show an inelastic response, the sintered bubbles display a high strength, stiffness, and toughness, while the mechanical properties of the calcined bubbles are intermediate between those of the as-assembled and the sintered bubbles. These microbubbles are incorporated into a polymer matrix using the layer-by-layer method (Fig. 11). The mechanical properties of the obtained polymer-bubble composites depend strongly on those of the individual bubbles while maintaining a low density for all three composites. Accordingly, it is meritorious that a variety of functional bubbles incorporated with versatile matrix components can efficiently tailor the mechanical properties of composite materials with designed functionalities.

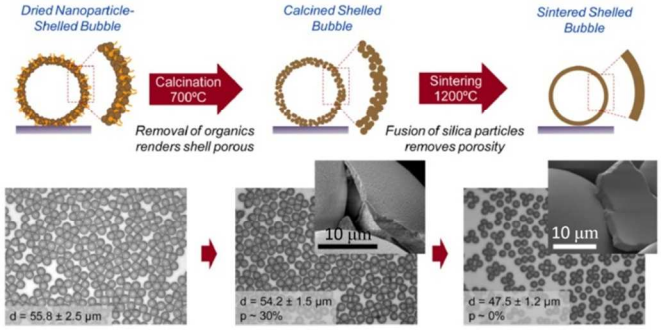

Fig. 10 Surface modification of nanoparticle-shelled microbubbles upon thermal treatment. The microbubbles were prepared by using the flow-focusing microfluidics. Modified and reprinted from ref. 86 with permission.

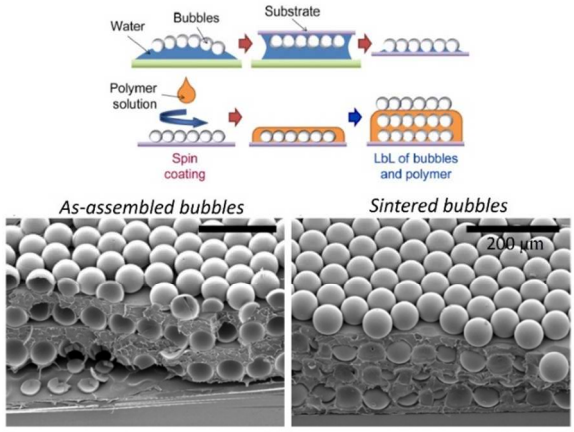

Fig. 11 Fabrication of microbubble-polymer composites whose mechanical properties depend on those of the microbubbles. Modified and reprinted from ref. 86 with permission.

Directed assembly of microbubbles stabilized by various types of particles can be used to produce three-dimensional nanostructured materials with tunable multi-functional properties. The stimuli-responsive feature of such functional materials stems from the characteristics of individual microbubbles used as a building block in the structure. For instance, a collection of microbubbles, of which the shell of each bubble was composed of magnetic particles and thermo-responsive fatty acid tubes, exhibited multi-responsiveness for thermo-, photo-, and magneto-stimuli.[54] The adsorption of graphene oxide to an emulsion interface leads to reduction of the interfacial tension due to its surface activity.[51, 124] Removal of the core fluid forms hollow capsules with a graphene oxide shell which possess excellent electrochemical properties when used as anode materials in a lithium-ion battery.[125] The graphene oxide bubbles can construct three-dimensional ordered networks in a liquid medium due to the low density of bubbles leading to compaction towards the interface.[126] A graphene oxide-based structured film which possesses electrically and mechanically improved properties is subsequently obtained by isolating the assembled bubbles via solvent drying.

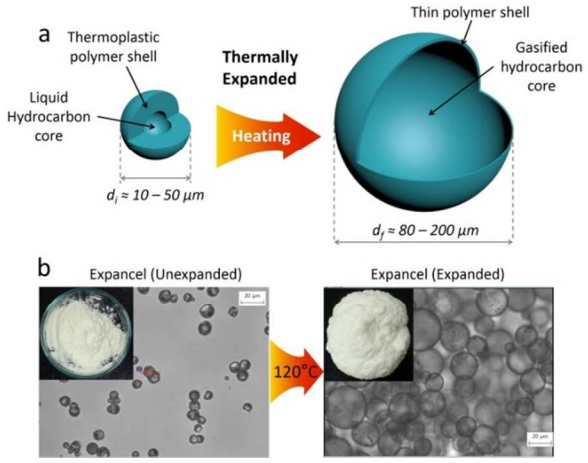

Fig. 12 (a) Schematic illustration of thermally expandable microcapsules (TEMs: expancel purchased from AkzoNobel). (b) Microscopic images of the TEMs before and after the thermal treatment. The insets show snapshots of the TEMs on a glass petri dish demonstrating the volume increase.

Thermally expandable microcapsules (TEMs) have been used as blowing agents or weight-reducing additives (Fig. 12).[47, 49, 127-130] Several tens of micron-sized polymer capsules containing hydrocarbon oil with a low boiling point have been prepared using suspension polymerization.[47, 49] In this process, a mixture of co-monomers and hydrocarbon (e.g., isobutene or isopentane) is vigorously suspended in an aqueous phase in the presence of appropriate stabilizers. Subsequent polymerization of the dispersed droplets leads to the formation of the double emulsion structure in which the polymer precipitates onto the emulsion-water interface due to its low solubility in the dispersed phase. This process results in a core/shell morphology where the hydrocarbon in the core is encapsulated by the polymer shell. Upon introducing thermal treatment at a certain critical temperature, the inner oil phase gasifies and thermally expands, significantly reducing the density. The mechanical and rheological properties of the shell polymer, such as the glass transition temperature and storage modulus, are important factors to determine the expandability and shrinkage of TEMs which can be controlled by the crosslinking extent in the polymer shell. The volatility of the encapsulated oil phase and gas permeability also significantly affect the performance of the TEMs. The surface of the TEMs can be further modified to control the onset time required for thermal expansion.[48, 131] For example, subjecting conducting polymer-coated TEMs to near-infrared irradiation leads to elevation of the local temperature. The resulting localized heating promotes rapid and efficient thermal expansion of TEMs compared to conventional bulk heating of bare TEMs. These TEMs incorporated with appropriate polymers and additives can be potentially applied for large-scale manufacturing processes such as injection molding or extrusion, enabling the fabrication of lightweight products in clothing, electronics, transportation, aerospace, and construction industries. The thermal responsibility feature of TEMs can be further exploited in minute actuation of nanoliter liquid volumes and flow control valves in microfluidics applications (Fig. 13).[132, 133] The

thermally induced volume increase of TEMs in a water-filled container with one open capillary channel displaces the channel with water at the expense of the volume change of the TEMs. Similarly, unexpanded TEMs confined in a microfluidics channel allow fluid flow to pass, whereas the expanded TEMs block the channel, impeding the flow.

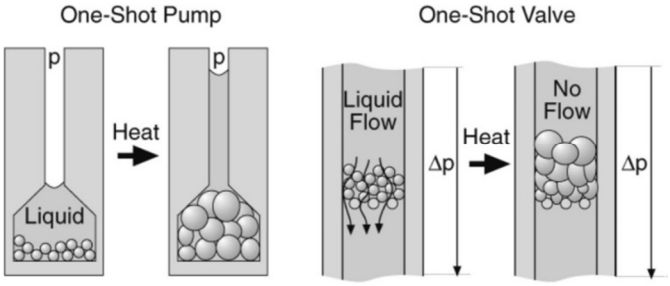

Fig. 13 Schematics of the minute actuation of nanoliter liquid volumes and flow control valves in microfluidic applications. Reprinted from ref. 133 with permission from The Royal Society of Chemistry.

Summary and Outlook

Considerable attention has been devoted to advanced applications of microbubbles for medical purposes and building blocks for hierarchical materials with versatile functionalities. The crucial factors in the microbubble generation are the controllability of size and productivity of the microbubbles. The microfluidic approach enables the generation of microbubbles with a high uniformity, where the size of the microbubbles can be readily controlled by the flow rates of input fluid streams and the geometry of microfluidic devices. In spite of the advantage of size uniformity, high yield production of microbubbles remains the most challenging issue in the application of microfluidic methods. Although the membrane emulsification technique offers a relatively high productivity due to the direct formation of emulsified bubbles in an aqueous phase that are forced through a porous membrane, the size uniformity should be improved for applications for highly structured materials and medical purposes. The inkjet printing method driven by the piezoelectric device can offer a promising route for achieving bubbles with good productivity and size uniformity. However, the selection of materials forming the bubble shell is strictly limited because single droplets produced by the inkjet method should undergo phase separation, leading to the formation of a core-shell structure in which the core liquid should be subsequently removed to produce hollow microbubbles. A new technique can be developed by combining microfluidics, membrane emulsification, and the inkjet method in which a dispersed phase (gas or liquid) is forced through a micro-nozzle system composed of hundreds of micro-holes with the same diameter on a flat surface of the micro-nozzle (Fig. 14). A piezoelectric device connected to the micro-nozzle creates pulses to the nozzle and each pulse leads to the formation of bubbles or liquid droplets with the same size upon providing a gas or a liquid mixture to the micro-nozzle. The gas bubbles or liquid droplets are then dispersed in a continuous fluid medium with appropriate stabilizers that flow along the nozzle surface. The size of the dispersed phase squeezed out of the multiple micro-holes can be additionally controlled via the shear stress of the continuous flow, interfacial tension, buoyancy force of the dispersed phase, and applied pressure of the input stream.

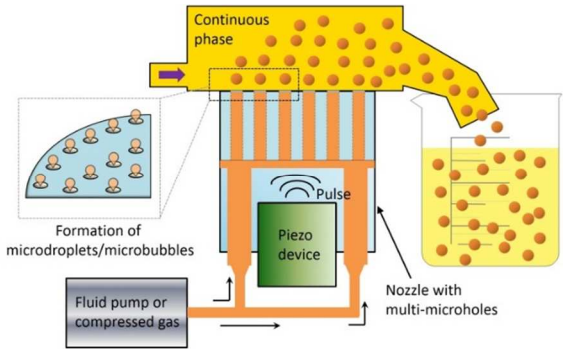

Fig. 14 Schematic of the proposed method for the generation of microbubbles with a narrow size distribution and a high productivity.

Applications of microbubbles have been extended to a variety of fields, such as food processing, water treatment, enhanced oil recovery, the study of geogas transportation, surface cleaning, medical purposes, and various functional materials. Another important application based on the microbubble system is the potential use of microbubbles as carriers of methane or syngas that can be used for biofuel production via a bio-catalytic process. For example, methanotrophs selectively convert methane to methanol, offering a promising route for cost-effective and one-step conversion of methane to liquid biofuel. A limiting factor in this bio-conversion system is the low solubility of methane gas in water and therefore, it is required to develop a process to effectively transfer the methane gas in an aqueous phase for bio-catalytic reactions. An enhanced efficiency of methane gas transfer can be achieved by generating microbubbles containing methane gas of which the stability can be readily controlled by using appropriate stabilizers.

Acknowledgements

We acknowledge financial support from the Engineering Research Center of Excellence Program of Korea Ministry of Science, ICT & Future Planning (MSIP)/National Research Foundation of Korea (NRF-2014-009799), and the New & Renewable Energy Core Technology Program of the Korea Institute of Energy Technology Evaluation and Planning (KETEP) and a grant from the Ministry of Trade, Industry & Energy, Republic of Korea (No. 20133030000090). We thank K. Kim for providing snapshots of the TEMs.

Notes and references

[a]Department of Chemical Engineering, Kyung Hee University, Yongin, 446-701, South Korea
[b]Department of Chemical and Biomolecular Engineering, University of Pennsylvania, Philadelphia, Pennsylvania, 19104, United States

Corresponding authors: Daeyeon Lee: (Tel) +1-215-573-4521, (email): daeyeon@seas.upenn.edu; Bum Jun Park: (Tel) +82-31-201-2429, (email) bjpark@khu.ac.kr

1. F. Kremkau, R. Gramiak, E. Carstensen, P. Shah and D. Kramer, *Am. J. Roentgenol.*, 1970, **110**, 177-183.
2. H. Feigenbaum, J. M. Stone, D. A. Lee, W. K. Nasser and S. Chang, *Circulation*, 1970, **41**, 615-621.
3. K. Ferrara, R. Pollard and M. Borden, *Biomed. Eng.*, 2007, **9**, 415-447.
4. K. Hettiarachchi, S. Zhang, S. Feingold, A. P. Lee and P. A. Dayton, *Biotechnol. Progr.*, 2009, **25**, 938-945.
5. J. L. Bull, *Expert Opinion*, 2007, **4**, 475-493.
6. I. Lentacker, S. C. De Smedt and N. N. Sanders, *Soft Matter*, 2009, **5**, 2161-2170.
7. S. Hernot and A. L. Klibanov, *Adv. Drug. Deliver. Rev.*, 2008, **60**, 1153-1166.
8. A. L. Klibanov, *Invest. Radiol.*, 2006, **41**, 354-362.
9. W. Song, H. Möhwald and J. Li, *Biomaterials*, 2010, **31**, 1287-1292.
10. K. Kooiman, M. R. Böhmer, M. Emmer, H. J. Vos, C. Chlon, W. T. Shi, C. S. Hall, S. H. P. M. de Winter, K. Schroën, M. Versluis, N. de Jong and A. van Wamel, *J. Control Release*, 2009, **133**, 109-118.
11. J. R. Lindner, *Nat. Rev. Drug. Discov.*, 2004, **3**, 527-533.
12. W. Song, Q. He, H. Möhwald, Y. Yang and J. Li, *J. Control Release*, 2009, **139**, 160-166.
13. Y. Liu, H. Miyoshi and M. Nakamura, *J. Control Release*, 2006, **114**, 89-99.
14. E. Barbarese, S.-Y. Ho, J. S. D'Arrigo and R. H. Simon, *J. Neuro Oncol.*, 1995, **26**, 25-34.
15. D. K. Brunk and D. A. Hammer, *Biophys. J.*, 1997, **72**, 2820.
16. J. S. D'arrigo, S.-Y. Ho and R. H. Simon, *Investig Radiol.*, 1993, **28**, 218-222.
17. N. G. Fisher, J. P. Christiansen, A. Klibanov, R. P. Taylor, S. Kaul and J. R. Lindner, *J. Am. Coll. Cardiol.*, 2002, **40**, 811-819.
18. P. Haag, F. Frauscher, J. Gradl, A. Seitz, G. Schäfer, J. R. Lindner, A. L. Klibanov, G. Bartsch, H. Klocker and I. E. Eder, *J. Steroid Biochem. Mol. Biol.*, 2006, **102**, 103-113.
19. S. Hodges and O. Jensen, *J. Fluid Mech.*, 2002, **460**, 381-409.
20. A. L. Klibanov, *Adv. Drug. Deliver. Rev.*, 1999, **37**, 139-157.
21. G. M. Lanza, K. D. Wallace, S. E. Fischer, D. H. Christy, M. J. Scott, R. L. Trousil, W. P. Cacheris, J. G. Miller, P. J. Gaffney and S. A. Wickline, *Ultrasound Med. Biol.*, 1997, **23**, 863-870.
22. J. R. Lindner, J. Song, J. Christiansen, A. L. Klibanov, F. Xu and K. Ley, *Circulation*, 2001, **104**, 2107-2112.
23. A. A. Rahim, S. L. Taylor, N. L. Bush, G. R. ter Haar, J. C. Bamber and C. D. Porter, *J. Gene Med.*, 2006, **8**, 1347-1357.
24. R. H. Simon, S.-Y. Ho, C. R. Perkins and J. S. D'arrigo, *Invest. Radiol.*, 1992, **27**, 29.
25. S. L. Taylor, A. A. Rahim, N. L. Bush, J. C. Bamber and C. D. Porter, *J. Gene Med.*, 2007, **9**, 77-87.
26. X. Wang, H.-D. Liang, B. Dong, Q.-L. Lu and M. J. Blomley, *Radiology*, 2005, **237**, 224-229.
27. G. E. Weller, E. Lu, M. M. Csikari, A. L. Klibanov, D. Fischer, W. R. Wagner and F. S. Villanueva, *Circulation*, 2003, **108**, 218-224.
28. G. E. Weller, M. K. Wong, R. A. Modzelewski, E. Lu, A. L. Klibanov, W. R. Wagner and F. S. Villanueva, *Cancer Res.*, 2005, **65**, 533-539.
29. K. Wei, A. R. Jayaweera, S. Firoozan, A. Linka, D. M. Skyba and S. Kaul, *Circulation*, 1998, **97**, 473-483.
30. T. Faez, M. Emmer, K. Kooiman, M. Versluis, A. F. van der Steen and N. de Jong, *IEEE T. Ultrason. Ferr.*, 2013, **60**.
31. K. Kooiman, H. J. Vos, M. Versluis and N. de Jong, *Adv. Drug Deliver. Rev.*, 2014, **72**, 28-48.
32. W. Jang, A. Nikolov and D. Wasan, *J. Food. Eng.*, 2006, **76**, 256-260.
33. R. Zúñiga and J. Aguilera, *Trends. Food. Sci. Tech.*, 2008, **19**, 176-187.
34. K. W. Soli, A. Yoshizumi, A. Motomatsu, M. Yamakawa, M. Yamasaki, T. Mishima, N. Miyaji, K.-I. Honjoh and T. Miyamoto, *Food. Control*, 2010, **21**, 1240-1244.
35. M. Shimoda, H. Ishikawa, T. Kawano and Y. Osajima, *J. Food. Sci.*, 1994, **59**, 231-232.
36. Y. Inatsu, T. Kitagawa, N. Nakamura, S. Kawasaki, D. Nei, M. L. Bari and S. Kawamoto, *Food. Sci. Technol. Res.*, 2011, **17**, 479-485.
37. D. Reay and G. Ratcliff, *Can. J. Chem. Eng.*, 1973, **51**, 178-185.
38. M. A. Malik, A. Ghaffar and S. A. Malik, *Plasma Sources Sci. T*, 2001, **10**, 82.
39. S. V. Bortkevitch, S. A. Kostrov, N. V. Savitsky and W. O. Wooden, U. S. Pat. No. 7,059,591, 2006.
40. R. W. Klusman, *Appl. Geochem.*, 2003, **18**, 1825-1838.
41. M. M. Monnin and J. L. Seidel, *Radiat. Meas.*, 1997, **28**, 703-712.
42. G. Etiope and S. Lombardi, *Geo*, 1996, **27**, 226-232.
43. A. Vàrhegyi, J. Hakl, M. Monnin, J. P. Morin and J. L. Seidel, *J. Appl. Geophys.*, 1992, **29**, 37-46.
44. C.-D. Ohl, M. Arora, R. Dijkink, V. Janve and D. Lohse, *Appl. Phys. Lett.*, 2006, **89**, 074102.
45. R. Dijkink and C.-D. Ohl, *Appl. Phys. Lett.*, 2008, **93**, 254107.
46. W. D. Song, M. H. Hong, B. Lukyanchuk and T. C. Chong, *J. Appl. Phys.*, 2004, **95**, 2952-2956.
47. Y. Kawaguchi, D. Ito, Y. Kosaka, M. Okudo, T. Nakachi, H. Kake, J. K. Kim, H. Shikuma and M. Ohshima, *Polym. Eng. Sci.*, 2010, **50**, 835-842.
48. A. Schmid, L. R. Sutton, S. P. Armes, P. S. Bain and G. Manfre, *Soft Matter*, 2009, **5**, 407-412.
49. M. Jonsson, O. Nordin, E. Malmström and C. Hammer, *Polymer*, 2006, **47**, 3315-3324.
50. A. R. Studart, U. T. Gonzenbach, I. Akartuna, E. Tervoort and L. J. Gauckler, *J. Mater. Chem.*, 2007, **17**, 3283-3289.
51. J. J. Shao, W. Lv and Q. H. Yang, *Adv. Mater.*, 2014, **26**, 5586–5612.
52. U. T. Gonzenbach, A. R. Studart, E. Tervoort and L. J. Gauckler, *Angew. Chem. Int. Ed.*, 2006, **45**, 3526-3530.

53. S. Lam, E. Blanco, S. K. Smoukov, K. P. Velikov and O. D. Velev, *J. Am. Chem. Soc.*, 2011, **133**, 13856-13859.
54. A.-L. Fameau, S. Lam and O. D. Velev, *Chem. Sci.*, 2013, **4**, 3874-3881.
55. E. Blanco, S. Lam, S. K. Smoukov, K. P. Velikov, S. A. Khan and O. D. Velev, *Langmuir*, 2013, **29**, 10019-10027.
56. S. M. Joscelyne and G. Trägårdh, *J. Food. Eng.*, 1999, **39**, 59-64.
57. E. Stride and M. Edirisinghe, *Soft Matter*, 2008, **4**, 2350-2359.
58. M. J. Borrelli, *Ultrason. Sonochem.*, 2012, **19**, 198-208.
59. F. Cavalieri, M. Ashokkumar, F. Grieser and F. Caruso, *Langmuir*, 2008, **24**, 10078-10083.
60. M. W. Grinstaff and K. S. Suslick, *P. Natl. Acad. Sci. USA*, 1991, **88**, 7708-7710.
61. Q. Xu, M. Nakajima, S. Ichikawa, N. Nakamura and T. Shiina, *Innov. Food. Sci. Emerg.*, 2008, **9**, 489-494.
62. Z. Yan, R. Bao, Y. Huang and D. B. Chrisey, *J. Phys. Chem. C*, 2010, **114**, 11370-11374.
63. B. Jiang, C. Gao and J. Shen, *Colloid. Polym. Sci.*, 2006, **284**, 513-519.
64. W. Cui, J. Bei, S. Wang, G. Zhi, Y. Zhao, X. Zhou, H. Zhang and Y. Xu, *J. Biomed. Mater. Res. B*, 2005, **73**, 171-178.
65. K. Bjerknes, P. Sontum, G. Smistad and I. Agerkvist, *Int. J. Pharm.*, 1997, **158**, 129-136.
66. P. Garstecki, I. Gitlin, W. DiLuzio, G. M. Whitesides, E. Kumacheva and H. A. Stone, *Appl. Phys. Lett.*, 2004, **85**, 2649-2651.
67. J. I. Park, Z. Nie, A. Kumachev and E. Kumacheva, *Soft Matter*, 2010, **6**, 630-634.
68. J.-H. Xu, R. Chen, Y.-D. Wang and G.-S. Luo, *Lab. Chip*, 2012, **12**, 2029-2036.
69. J. Xu, S. Li, Y. Wang and G. Luo, *Appl. Phys. Lett.*, 2006, **88**, 133506.
70. J. Wan, A. Bick, M. Sullivan and H. A. Stone, *Adv. Mater.*, 2008, **20**, 3314-3318.
71. M. H. Lee and D. Lee, *Soft Matter*, 2010, **6**, 4326-4330.
72. P. Garstecki, M. J. Fuerstman, H. A. Stone and G. M. Whitesides, *Lab. Chip*, 2006, **6**, 437-446.
73. E. Talu, K. Hettiarachchi, R. L. Powell, A. P. Lee, P. A. Dayton and M. L. Longo, *Langmuir*, 2008, **24**, 1745-1749.
74. E. Talu, M. M. Lozano, R. L. Powell, P. A. Dayton and M. L. Longo, *Langmuir*, 2006, **22**, 9487-9490.
75. J. Wan and H. A. Stone, *Soft Matter*, 2010, **6**, 4677-4680.
76. E. Castro-Hernández, W. van Hoeve, D. Lohse and J. M. Gordillo, *Lab. Chip*, 2011, **11**, 2023-2029.
77. J. I. Park, E. Tumarkin and E. Kumacheva, *Macromol. Rapid. Comm.*, 2010, **31**, 222-227.
78. K. Hettiarachchi, E. Talu, M. L. Longo, P. A. Dayton and A. P. Lee, *Lab. Chip*, 2007, **7**, 463-468.
79. Y. Shen, M. L. Longo and R. L. Powell, *J. Colloid. Interf. Sci.*, 2008, **327**, 204-210.
80. B. Dollet, W. van Hoeve, J.-P. Raven, P. Marmottant and M. Versluis, *Phys. Rev.Lett.*, 2008, **100**, 034504.
81. J. I. Park, A. Saffari, S. Kumar, A. Günther and E. Kumacheva, *Ann. Rev. Mater. Res.*, 2010, **40**, 415-443.
82. J. I. Park, D. Jagadeesan, R. Williams, W. Oakden, S. Chung, G. J. Stanisz and E. Kumacheva, *Acs. Nano*, 2010, **4**, 6579-6586.
83. T. Brugarolas, B. J. Park, M. H. Lee and D. Lee, *Adv. Funct. Mater.*, 2011, **21**, 3924-3931.
84. J. I. Park, Z. Nie, A. Kumachev, A. I. Abdelrahman, B. P. Binks, H. A. Stone and E. Kumacheva, *Angew. Chem. Int. Ed.*, 2009, **121**, 5404-5408.
85. M. H. Lee, V. Prasad and D. Lee, *Langmuir*, 2009, **26**, 2227-2230.
86. T. Brugarolas, D. S. Gianola, L. Zhang, G. M. Campbell, J. L. Bassani, G. Feng and D. Lee, *ACS Appl. Mater. Interfaces*, 2014, **6**, 11558-11572.
87. V. Schröder, O. Behrend and H. Schubert, *J. Colloid. Interf. Sci.*, 1998, **202**, 334-340.
88. M. Kukizaki and M. Goto, *Colloid Surface A*, 2007, **296**, 174-181.
89. M. Kukizaki and T. Wada, *Colloid Surface A*, 2008, **317**, 146-154.
90. S. M. Joscelyne and G. Trägårdh, *J. Membrane. Sci.*, 2000, **169**, 107-117.
91. M. R. Böhmer, R. Schroeders, J. A. M. Steenbakkers, S. H. P. M. de Winter, P. A. Duineveld, J. Lub, W. P. M. Nijssen, J. A. Pikkemaat and H. R. Stapert, *Colloid. Surface. A*, 2006, **289**, 96-104.
92. U. Farook, E. Stride, M. J. Edirisinghe and R. Moaleji, *Med Bio Eng Comput*, 2007, **45**, 781-789.
93. U. Farook, H. Zhang, M. Edirisinghe, E. Stride and N. Saffari, *Med. Eng. Phys.*, 2007, **29**, 749-754.
94. Z. Ahmad, H. Zhang, U. Farook, M. Edirisinghe, E. Stride and P. Colombo, *J. R. S. Interface*, 2008, **5**, 1255-1261.
95. M. Motornov, Y. Roiter, I. Tokarev and S. Minko, *Prog. Polym. Sci.*, 2010, **35**, 174-211.
96. W. Song, Y. Yang, H. Moehwald and J. Li, *Soft Matter*, 2011, **7**, 359-362.
97. H. A. Jerri, R. A. Dutter and D. Velegol, *Soft Matter*, 2009, **5**, 827-834.
98. V. Kozlovskaya, S. Ok, A. Sousa, M. Libera and S. A. Sukhishvili, *Macromolecules*, 2003, **36**, 8590-8592.
99. Q. He, W. Song, H. Möhwald and J. Li, *Langmuir*, 2008, **24**, 5508-5513.
100. M. A. Pechenkin, H. Möhwald and D. V. Volodkin, *Soft Matter*, 2012, **8**, 8659-8665.
101. D. Lensen, D. M. Vriezema and J. van Hest, *Macromol. Biosci.*, 2008, **8**, 991-1005.
102. B. G. De Geest, N. N. Sanders, G. B. Sukhorukov, J. Demeester and S. C. De Smedt, *Chem. Soc. Rev.*, 2007, **36**, 636-649.
103. O. Shchepelina, I. Drachuk, M. K. Gupta, J. Lin and V. V. Tsukruk, *Adv. Mater.*, 2011, **23**, 4655-4660.
104. Z. Wang, Z. Feng and C. Gao, *Chem. Mater.*, 2008, **20**, 4194-4199.
105. G. B. Sukhorukov, E. Donath, S. Davis, H. Lichtenfeld, F. Caruso, V. I. Popov and H. Möhwald, *Polym. Advan. Technol*, 1998, **9**, 759-767.
106. B. S. Murray, *Curr. Opin. Colloid In.*, 2007, **12**, 232-241.
107. A. L. Fameau, A. Saint-Jalmes, F. Cousin, B. Houinsou Houssou, B. Novales, L. Navailles, J. Emile, F. Nallet, C. Gaillard, F. Boué and J. P. Douliez, *Angew. Chem. Int. Ed.*, 2011, **50**, 8264-8269.
108. A. Carl and R. von Klitzing, *Angew. Chem. Int. Ed.*, 2011, **50**, 11290-11292.
109. B. S. Murray, E. Dickinson, C. K. Lau, P. V. Nelson and E. Schmidt, *Langmuir*, 2005, **21**, 4622-4630.
110. R. Ettelaie, E. Dickinson, Z. Du and B. S. Murray, *J. Colloid. Interf. Sci.*, 2003, **263**, 47-58.

111. I. M. Lifshitz and V. V. Slyozov, *J. Phys. Chem. Solids*, 1961, **19**, 35-50.
112. C. Wagner, *Z. Elektrochem.*, 1961, **65**, 581-591.
113. A. S. Kabalnov and E. D. Shchukin, *Adv. Colloid Interface*, 1992, **38**, 69-97.
114. J. Marqusee and J. Ross, *J. Chem. Phys.*, 1984, **80**, 536-543.
115. M. B. J. Meinders, W. Kloek and T. van Vliet, *Langmuir*, 2001, **17**, 3923-3929.
116. H. W. Yarranton and J. H. Masliyah, *J. Colloid. Interf. Sci.*, 1997, **196**, 157-169.
117. E. Dickinson, R. Ettelaie, B. S. Murray and Z. Du, *J. Colloid. Interf. Sci.*, 2002, **252**, 202-213.
118. W. Kloek, T. van Vliet and M. Meinders, *J. Colloid. Interf. Sci.*, 2001, **237**, 158-166.
119. Q. Xu, M. Nakajima, S. Ichikawa, N. Nakamura, P. Roy, H. Okadome and T. Shiina, *J. Colloid. Interf. Sci.*, 2009, **332**, 208-214.
120. T. Kostakis, R. Ettelaie and B. S. Murray, *Langmuir*, 2006, **22**, 1273-1280.
121. A. B. Subramaniam, C. Mejean, M. Abkarian and H. A. Stone, *Langmuir*, 2006, **22**, 5986-5990.
122. A. B. Subramaniam, M. Abkarian and H. A. Stone, *Nat. Mater*, 2005, **4**, 553-556.
123. Y. Xia and G. M. Whitesides, *Annu. Rev. Mater. Sci.*, 1998, **28**, 153-184.
124. J. Kim, L. J. Cote, F. Kim, W. Yuan, K. R. Shull and J. Huang, *J. Am. Chem. Soc.*, 2010, **132**, 8180-8186.
125. P. Guo, H. Song and X. Chen, *J. Mater. Chem.*, 2010, **20**, 4867-4874.
126. S. H. Lee, H. W. Kim, J. O. Hwang, W. J. Lee, J. Kwon, C. W. Bielawski, R. S. Ruoff and S. O. Kim, *Angew. Chem. Int. Ed.*, 2010, **122**, 10282-10286.
127. M. Jonsson, O. Nordin, A. L. Kron and E. Malmström, *J. Appl. Polym. Sci.*, 2010, **117**, 384-392.
128. D. S. J. Morehouse and R. J. Tetreault, U.S. Pat. 3,615,972, 1971.
129. H. Ogawa, A. Ito, K. Taki and M. Ohshima, *J. Appl. Polym. Sci.*, 2007, **106**, 2825-2830.
130. Y. Kawaguchi and T. Oishi, *J. Appl. Polym. Sci.*, 2004, **93**, 505-512.
131. H. E. Cingil, J. A. Balmer, S. P. Armes and P. S. Bain, *Polym. Chem.*, 2010, **1**, 1323-1331.
132. S. K. Sia and G. M. Whitesides, *Electrophoresis*, 2003, **24**, 3563-3576.
133. P. Griss, H. Andersson and G. Stemme, *Lab. Chip*, 2002, **2**, 117-120.

Table of contents entry

In this review, we discuss the controlled stability of microbubbles, recent developments in a variety of microbubble preparation techniques, and applications of bubbles for medicine and functional materials.

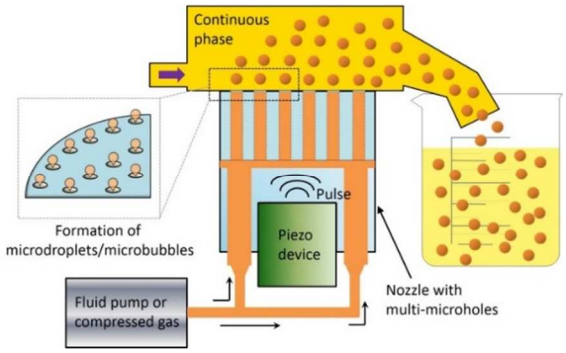

Biography:

Mina Lee is a graduate student in the Department of Chemical Engineering at Kyung Hee University under the supervision of Prof. B. J. Park. She earned her B.S in Environmental Science at the Hankuk University of Foreign Studies in 2013. Her research interests focus on assemblies of colloidal particles and microfluidic systems.

Eun Yeol Lee obtained his Ph.D. in 1995 from Seoul National University. He visited Microbiology Institute at Goettingen University (Germany), Industrial Microbiology and Food Biotechnology Institute at Wageningen University (The Netherlands) and Biomedical Engineering Department at Cornell University (USA) as a visiting scholar. Currently, he is a professor of Chemical Engineering Department at Kyung Hee University. His research interests are Protein/Metabolic Engineering, Nanobiocatalysis, and Biorefinery for the production of Biofuels, Biochemicals and Biopolymers from lignocellulosic biomass, macro-/microalgae and methane.

Daeyeon Lee received his B.S. in Chemical Engineering from Seoul National University in 2001 and received his Ph.D. in Chemical Engineering at MIT in 2007. After his postdoctoral fellowship at Harvard University, Daeyeon joined the University of Pennsylvania in 2009 and is currently Associate Professor of Chemical and Biomolecular Engineering. Daeyeon's research interests include structure-property relationship of nanoparticle assemblies, interfacial behavior of Janus particles and microfluidic fabrication of functional structures. Daeyeon has won numerous awards including the 2010 Victor K. LaMer Award, NSF CAREER Award, 2013 3M Nontenured Faculty Award, 2013 AIChE NSEF Young Investigator Award and 2014 Unilever Award for Outstanding Young Investigator in Colloid & Surfactant Science.

Bum Jun Park obtained his Ph.D. in 2010 at the University of Delaware. After spending two years as a postdoctoral researcher at the University of Pennsylvania, he is currently an assistant professor in the Department of Chemical Engineering at Kyung Hee University. His research interests focus on interaction and microstructure of various functional particles at fluid-fluid interfaces.